2018

# Towards characterizing LNAPL remediation endpoints

Kaveh Sookhak Lari
*Edith Cowan University*

John L. Rayner

Greg B. Davis



10.1016/j.jenvman.2018.07.041
Sookhak Lari, K., Rayner, J. L., & Davis, G. B. (2018). Towards characterizing LNAPL remediation endpoints. Journal of Environmental Management, 224, 97-105. Available here

Journal of Environmental Management 224 (2018) 97–105

Contents lists available at ScienceDirect

Journal of Environmental Management

journal homepage: www.elsevier.com/locate/jenvman

# Towards characterizing LNAPL remediation endpoints

Kaveh Sookhak Lari[a,b,c,*], John L. Rayner[a,b], Greg B. Davis[a,b,d]

[a] CSIRO Land and Water, Private Bag No. 5, Wembley, WA, 6913, Australia
[b] Cooperative Research Centre for Contamination Assessment and Remediation of the Environment (CRC CARE), Australia
[c] School of Engineering, Edith Cowan University, 270 Joondalup Drive, Joondalup, WA, 6027, Australia
[d] School of Earth Sciences, The University of Western Australia, 35 Stirling Highway, Crawley, WA, 6009, Australia

ARTICLE INFO

*Keywords:*
LNAPL remediation
Multi-phase
Multi-component
Simulation
Endpoint

ABSTRACT

Remediating sites contaminated with light non-aqueous phase liquids (LNAPLs) is a demanding and often prolonged task. It is vital to determine when it is appropriate to cease engineered remedial efforts based on the long-term effectiveness of remediation technology options. For the first time, the long term effectiveness of a range of LNAPL remediation approaches including skimming and vacuum-enhanced skimming each with and without water table drawdown was simulated through a multi-phase and multi-component approach. LNAPL components of gasoline were simulated to show how component changes affect the LNAPL's multi-phase behaviour and to inform the risk profile of the LNAPL. The four remediation approaches along with five types of soils, two states of the LNAPL specific mass and finite and infinite LNAPL plumes resulted in 80 simulation scenarios. Effective conservative mass removal endpoints for all the simulations were determined. As a key driver of risk, the persistence and mass removal of benzene was investigated across the scenarios. The time to effectively achieve a technology endpoint varied from 2 to 6 years. The recovered LNAPL in the liquid phase varied from 5% to 53% of the initial mass. The recovered LNAPL mass as extracted vapour was also quantified. Additional mass loss through induced biodegradation was not determined. Across numerous field conditions and release incidents, graphical outcomes provide conservative (i.e. more prolonged or greater mass recovery potential) LNAPL remediation endpoints for use in discussing the halting or continuance of engineered remedial efforts.

## 1. Introduction

The release of hazardous organic chemicals including light non-aqueous phase liquids (LNAPLs, such as petroleum hydrocarbons) into the vadose zone and groundwater is a significant environmental concern due to its potential adverse effects (Davis et al., 2009). LNAPLs form an immiscible liquid plume in the vadose zone and across the capillary fringe (Lenhard et al., 2018). This induces the partitioning of compounds into gaseous and aqueous phase exposure pathways (Lang et al., 2009; Rivett, 2014; Davis et al., 2005). An initial critical step for remediation of an impacted site is to recover LNAPL through appropriate remediation techniques. To enhance removal of LNAPL mass, various forms of recovery methods may be applicable. These include air, water or solvent flushing or single, dual and multi-phase purging of LNAPL, soil gas and water (Khan et al., 2004; Davis et al., 2013) (Johnston and Trefry, 2009). However, as the dynamics of LNAPL in the subsurface is a function of different parameters (including geo-physical properties of the porous media and the distribution and composition of the LNAPL itself), the feasibility and effectiveness of each (or any combination) of the aforementioned techniques for a particular site is a question to be answered prior to any remedial effort.

After early and primary stages of pumping LNAPL out of an aquifer, a considerable amount of LNAPL may still remain in the subsurface (Lenhard et al., 2018). This is mostly due to the dominance of capillary forces and therefore, a secondary or tertiary recovery effort may be required to remove less-mobile LNAPL (Hernández-Espriú et al., 2012). These may include application of dual and multi-phase recovery techniques. However, information and data in the literature with respect to how to best operate recovery methods to gain an optimum long-term LNAPL recovery are not extensive (Jeong and Charbeneau, 2014; Johnston and Trefry, 2009).

Analytical models have been used to estimate long-term LNAPL mass recovered (in the liquid phase) through multi-phase recovery techniques (Charbeneau et al., 2000). A number of studies have explored the level of LNAPL mass removal required to significantly reduce the net flux dissolved in groundwater (Huntley and Beckett, 2002;

* Corresponding author.CSIRO Land and Water, Private Bag No. 5, Wembley, WA, 6913, Australia.
*E-mail address:* kaveh.sookhaklari@csiro.au (K. Sookhak Lari).

https://doi.org/10.1016/j.jenvman.2018.07.041
Received 27 February 2018; Received in revised form 3 July 2018; Accepted 14 July 2018
Available online 20 July 2018

DiFilippo and Brusseau, 2008; Johnston et al., 2013). None of these studies indicate the extent of mass removal that may be achievable. Also, the rate of mass removal during active remediation is likely to decrease over time and may become comparable or less than that due to natural mass loss and biodegradation processes – referred to as LNAPL natural source zone depletion (NSZD) (Garg et al., 2017; Chaplin et al., 2002; Johnson et al., 2006). Such an occurrence would be a trigger to consider NSZD as an ongoing management option, compared to continued engineered mass removal efforts. Rates for NSZD via subsurface partitioning and biodegradation are increasingly reported in the literature (Barry et al., 2002; Mulligan and Yong, 2004; Prommer et al., 2000). To enable the comparison with NSZD mass removal rates, rates of mass LNAPL recovery via engineering approaches need to be better estimated over prolonged periods to yield feasible endpoints.

Numerical studies have partially addressed the quantitative endpoint problem. Gabr et al. (2013) applied the Bioslurp model and determined 4.5 years as an endpoint to a multi-phase recovery plan. Skinner (2013) conducted a similar numerical study to predict the endpoint of a skimming approach. Hernández-Espriú et al. (2012) used the API model (a one-dimensional quasi-analytical single component LNAPL model) to investigate the long term (3 year) performance of several multi-phase recovery approaches. Jeong and Charbeneau (2014) presented another analytical model (named LDRM) to study certain types of LNAPL recovery methods. However, no extensive investigation of the effective LNAPL mass removal endpoint has been undertaken taking account of compositional changes within a multi-phase simulation strategy (Sookhak Lari et al., 2018). Such an approach is required to best capture the physics of three-phase (NAPL, water, and gas) subsurface transport and the partitioning and fate of LNAPL components. The components have different risk profiles, and depletion of components alters the physical properties of the LNAPL itself.

A list of recent multi-phase and multi-component simulation studies using multi-phase numerical codes can be found in Sookhak Lari et al. (2016a). The serial-processing code TMVOC (which is a member of the TOUGH2 family of simulators (Pruess and Battistelli, 2002)) is able to represent key features of multi-component LNAPL transport and partitioning in porous media. This code has also been presented in a parallel version (TMVOC-MP) to cope with more complicated problems in terms of geometry, mesh resolution and the number of partitioning compounds in LNAPL (Zhang et al., 2007). However, multi-phase numerical simulators (including TMVOC) have not been used with component partitioning to determine an effective endpoint to field-scale LNAPL remedial approaches (Sookhak Lari et al., 2018).

Recently TMVOC-MP was verified on a CRAY supercomputer through a three-dimensional multi-phase and multi-component simulation of various multi-phase LNAPL remediation approaches applied sequentially over a 78-day period (Sookhak Lari et al., 2018). Here we use the same modelling framework to numerically assess the long term performance of various LNAPL remediation approaches including skimming alone and skimming with vacuum enhanced extraction, and with both these methods applied with and without water table drawdown. We consider five types of soils including sand, loamy sand, loam, silt and silty clay - spanning over three orders of magnitude in permeability with significantly different soil moisture characteristic curves over this range. Both finite and infinitely extended LNAPL plumes were assumed and for each, a high and a low initial LNAPL specific mass is considered. The superposition and performance of more than one recovery wells are not addressed here. Biodegradation is excluded and therefore, the results represent a conservative (upper limit) endpoint, since by excluding biodegradation processes, greater LNAPL mass will be preserved in the subsurface, creating predictions of longer time periods of potentially greater mass recovery to achieve an asymptotic LNAPL recovery endpoint for the cases studied here.

This is the first time an approach combining multiphase partitioning and phase mobility has been investigated to determine the physical (conservative) endpoints for LNAPL remedial techniques. This has been established on a supercomputer to address 80 scenarios of LNAPL recoverability to provide simulations in a new nomograph style for adoption by industry and regulators. Overall, these novel outcomes allow quantitative consideration of upper-limit endpoints as criteria by which remedial efforts might be halted or continued at LNAPL impacted sites.

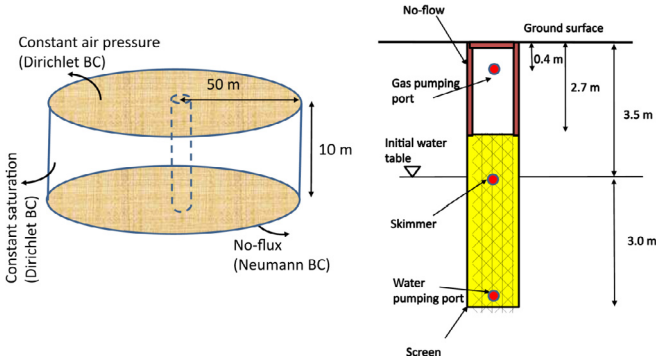


**Fig. 1.** The simulation domain and the boundary conditions (left); The recovery well configuration (right).

## 2. Modelling scenarios

### 2.1. Site layout and soil/aquifer properties

We consider an area 100 m in diameter and 10 m in depth (Fig. 1 left) with an initial water table elevation 3.5 m below the surface. A multi-phase recovery well is located at the centre (Fig. 1 right). We consider five types of soils introduced in Table 1 (Carsel and Parrish, 1988). They include sand, loamy sand, loam, silt and silty clay and span over three orders of magnitude with respect to the soil permeability. Also the van Genuchten parameters for the soils are adopted from Carsel and Parrish (1988) which shows the diversity in their soil moisture characteristic curves.

### 2.2. Initial LNAPL characteristics and distribution

LNAPL gasoline was considered, due to the global abundance of its release incidents and also since it includes a wide range of compounds with very different partitioning attributes and risk profiles (Lekmine et al., 2017; Vasudevan et al., 2016; Sookhak Lari et al., 2016b). Several studies have reported the subsurface composition of gasoline (GSI Environmental Inc., 2012; Kaplan et al., 1997; Lekmine et al., 2017). Here we use the reported composition for a weathered gasoline in Sookhak Lari et al. (2016b). Major components in the gasoline were bundled into 7 representative groups, as introduced in Table 2 (Lekmine et al., 2017). The composition and thermo-physical properties of these groups are reported in Table 3.

We consider two types of architecture for the LNAPL plume; the Finite case (FIN) and the Infinite case (INF). For the FIN cases, 4945 kg and 24728 kg of mass released over a circle around the well with a

**Table 1**
Soils used for the simulations and their hydraulic properties; k is the permeability, K is the hydraulic conductivity and n and α are the van Genuchten water retention parameters (Carsel and Parrish, 1988).

| ID | Soil | k ($m^2$) | K (cm/s) | n | α (1/m) |
|---|---|---|---|---|---|
| S1 | Sand | $8.25 \times 10^{-12}$ | $8.25 \times 10^{-3}$ | 2.68 | 14.5 |
| S2 | Loamy sand | $4.05 \times 10^{-12}$ | $4.05 \times 10^{-3}$ | 2.28 | 12.4 |
| S3 | Loam | $2.89 \times 10^{-13}$ | $2.89 \times 10^{-4}$ | 1.56 | 3.6 |
| S4 | Silt | $6.94 \times 10^{-14}$ | $6.94 \times 10^{-5}$ | 1.37 | 1.6 |
| S5 | Silty clay | $5.56 \times 10^{-15}$ | $5.56 \times 10^{-6}$ | 1.09 | 0.5 |

**Table 2**
Abbreviations used in this study.

| Abbreviation | Description | Abbreviation | Description |
|---|---|---|---|
| SKM or SKIM | Skimming | BEN | Benzene |
| SKV or SKIMVAP | Skimming + vapour extraction | TOL | Toluene |
| SKW or SKIMWAT | Skimming + water table drawdown | XYL | Xylene |
| SKVW or SKIMVAP-WAT | Skimming + vapour extraction + water table drawdown | ETB | Ethylbenzene |
| INF | Infinite LNAPL plume | TMB | Trimethylbenzene |
| FIN | Finite LNAPL plume | NC46 | nC4-nC6 |
| S# | Soil number# | NC711 | nC7-nC11 |
| H/L | High/Low LNAPL specific mass | | |

**Table 3**
Fraction of the representative groups in the simulated LNAPL plus their molecular weight ($M_w$), mole-averaged vapour pressure (V. pres.) and water solubility (Sookhak Lari et al., 2016b).

| | $M_W$ | Mole % | Mass % | V. Press (*Pa*) | Solubility (*mole/mole*) |
|---|---|---|---|---|---|
| BEN | 78.11 | 1.16 | 0.88 | $1.26 \times 10^4$ | $40.6 \times 10^{-5}$ |
| TOL | 92.14 | 15.17 | 13.61 | $3.79 \times 10^3$ | $10.69 \times 10^{-5}$ |
| XYL | 106.16 | 16.14 | 16.68 | $1.06 \times 10^3$ | $2.91 \times 10^{-5}$ |
| ETB | 106.17 | 2.84 | 2.94 | $1.77 \times 10^3$ | $3.12 \times 10^{-5}$ |
| TMB | 240.35 | 5.16 | 12.08 | 287 | $0.47 \times 10^{-5}$ |
| NC46 | 75.25 | 32.14 | 23.55 | $5.64 \times 10^4$ | $0.73 \times 10^{-5}$ |
| NC711 | 114.31 | 27.18 | 30.26 | $1.91 \times 10^3$ | $0.03 \times 10^{-5}$ |

radius of 15 m for H and L cases respectively (specific mass of 7 kg/m$^2$ (L) and 35 kg/m$^2$ (H) at the end of the release). The system was then simulated to allow redistribution over 1000 days to form a quasi-steady LNAPL plume. For the INF cases, Fig. 2 shows the equilibrium LNAPL profiles for both L and H (specific mass of 7 kg/m$^2$ (L) and 35 kg/m$^2$ (H)) throughout the entire domain (initial condition) and at the outer boundary of Dirichlet type, prior to simulation of the application of remedial efforts.

Charbeneau et al. (2000) stated that if the equilibrium ratio (the ratio of the radius of recovery of the well to the free LNAPL thickness in the well) of a plume is much larger than 10, the assumption of vertical equilibrium in the LNAPL profile is justified. Such a condition might be considered to be the case for an infinite plume. Alternatively, the outer boundary condition we applied for the infinite plume yields a natural tendency for an inwards flux of the LNAPL towards the recovery well, following any LNAPL mass recovered from the well. This in practice mimics a recovery well in a plume caused by an ongoing and continuous release of LNAPL.

Finite plumes exist in reality. Even for extremely large LNAPL plumes, a network of recovery wells (with smaller radii of capture) are usually used to access a larger plume effectively via a number of sub-plumes (Charbeneau et al., 2000).

### 2.3. Remediation scenarios and parameters

Skimming is conducted through a port located close to the water table and adjustable for different recovery schemes based on the elevation of the maximum LNAPL saturation. Vapour extraction is conducted through a port 0.4 m below the surface (for methods including vacuum-enhanced recovery) and groundwater is pumped out through a port 3.0 m below the initial water table (for methods including water table drawdown). The well cap and wall are isolated down to 2.7 m below the surface. The following four recovery approaches are simulated; skimming, skimming enhanced with vapour extraction (vacuum-enhanced skimming), skimming enhanced with water table drawdown and skimming enhanced with both vapour extraction and water table drawdown. As we use a number of abbreviations to call several cases studied here, a list of the abbreviations used in this study is presented in Table 2.

The water table drawdown technique comprises pumping water at 5 m$^3$/day. Vacuum-enhanced recovery is simulated by pumping 5 l/s of air out of the well. These pumping rates were chosen after trial simulations to ensure in the majority of cases that we were able to produce the desired water and soil gas extraction rates for the duration of simulations. Also in choosing these values, we considered previous field trial conditions for the same remedial techniques (Johnston et al., 2001).

The combination of five soils, two LNAPL plume architectures, two specific masses and the four remediation methods indicated here forms 80 simulation cases as shown in Fig. 3.

## 3. Governing equations and computational resources

TMVOC-MP is the primary code used for the simulations reported here (Pruess and Battistelli, 2002). The code assumptions have been revisited through simulations of pilot, meso and field scale problems (Sookhak Lari et al., 2015; Lekmine et al., 2017; Sookhak Lari et al., 2018).

The integral mass conservation equation in TMVOC-MP is

$$\frac{d}{dt}\int_{V_n} M^K dV_n = \int_{\Gamma_n} F^K \cdot n d\Gamma_n + \int_{V_n} q^K dV_n \quad (1)$$

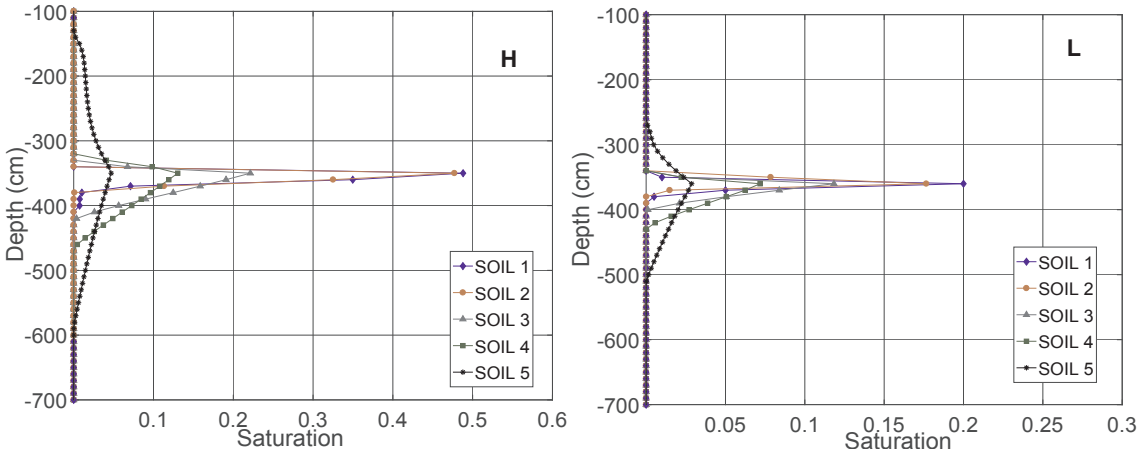


**Fig. 2.** LNAPL distribution profiles for the INF cases, various soils and specific masses. 'H' and 'L' indicate high and low specific mass (mass released per unit surface) cases. The profiles are after 1000 days of simulated natural redistribution prior to remedial efforts.

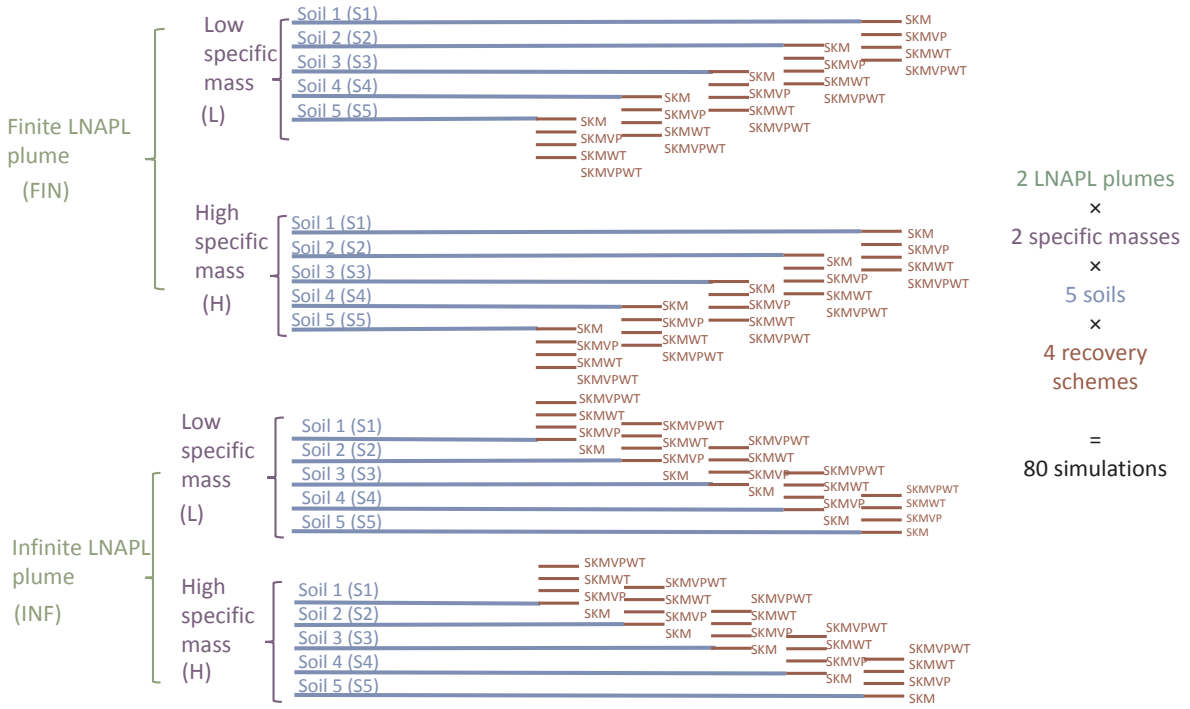


**Fig. 3.** The matrix of simulations conducted. Abbreviations are introduced in Table 2.

where *dVn* represents an arbitrary subdomain, $\Gamma_n$ is the surface of this subdomain, $M^K$ is the mass, F is the mass flux, $q$ is the sink/source term and n shows the normal vector on the surface element. Here, $K = 1, \ldots, NK$, where $NK$ is the number of components under study. The advective mass flux is

$$F^K = \sum_{\beta} X_{\beta} x F_{\beta} \tag{2}$$

in which

$$F_{\beta} = -k\frac{k_{r\beta}\rho_{\beta}}{\mu_{\beta}}(\nabla P_{\beta} - \rho_{\beta} g) \tag{3}$$

and $X_{\beta}$ is the molar fraction of component $K$ in phase $\beta$. Here, $k$ and $k_{r\beta}$ are the absolute and relative permeability (to phase $\beta$), $\mu$ represents the dynamic viscosity and $P$ is the total pressure. The vector g is gravitational acceleration. Relative permeability and capillary pressure parameters applied are introduced in Table (1) (Carsel and Parrish, 1988; Parker et al., 1987). For the capillary head h [L],

$$\frac{S_j^{ij} - S_m}{1 - S_m} = [1 + (\alpha_{ij} h)^n]^{-m},\ i, j = G, Aq, N,\ i \neq j \tag{4}$$

where $S_j^{ij}$ represents the effective wetting phase fluid saturation and $S_m$ is the irreducible saturation (of the wetting phase). The mesh comprises 100 × 146 cells in depth-wise and radial direction respectively. The evenly-distributed cells in depth each has a height of 10 cm. The radial dimension of the cells varies from 20 cm (near the well) to 60 cm (near the outer boundary). The boundary condition at the surface is atmospheric pressure (except for the no-flow condition at the well cap). The outer boundary condition is of Dirichlet type with constant saturation (shown in Fig. 1 for the INF cases).

We ran the simulations on a high performance computing facility, the Magnus Cray XC40 supercomputer (Intel Xeon Haswell processor cores) located at the Pawsey Supercomputing Centre in Perth, Australia. Each node in this machine consists of 24 cores. The simulations used almost $5.1 \times 10^4$ of CPU hours. More details on the simulation procedure can be found in Sookhak Lari et al. (2018).

We simulated the progress of LNAPL mass removal from the well using the four recovery methods for 3 + years. Due to the variations in the near-well LNAPL saturation during the simulations, continuous tracking was undertaken to adjust the level of the skimming port to maximise the LNAPL volumetric recovery rate. Also sensitivity analysis for the convergence error criterion and the mesh resolution were performed for selected cases.

## 4. Simulations and results

### 4.1. The endpoints

Figs. 4 and 5 include the results for the LNAPL recovery rates in the liquid phase for the H and L cases respectively. We discuss the INF simulations first (the dashed lines) and then the FIN cases.

#### 4.1.1. The infinite LNAPL plume

Except for L S4, L S5 and to some extent H S5 (Figs. 4 and 5), it is seen that the LNAPL volumetric recovery rate effectively asymptotes to certain values after almost $10^7$ s (115 days). The asymptotic values are around 1–30 l/day for H cases (except S5) and 0.10–8.0 l/day for L cases (except S5). The asymptotic values for the recovery rate in S5 are around two orders of magnitude lower (i.e., 0.004–0.04 l/day). This can be explained by reference to Fig. 2, whereby the van Genuchten parameters for such a tight soil distribute the NAPL mass over a greater vertical depth across the water table zone. In the case of S5, this is quite significant leading to a large portion of the LNAPL becoming immobile. For L S4 and L S5 the mass removal rates first decrease rapidly and then start to increase again. This is in response to the lower available mobile LNAPL mass in these low permeability soils. The delayed increase in mass recovery rates is because over time the radius of recovery expands to access the infinitely available LNAPL mass beyond the immediate limited effective radius of the well over the initial period.

For the more permeable soils (e.g., S1 and S2 cases), vacuum-enhanced recovery has a positive long term effect in comparison to skimming alone. However, the less permeable soils show a different behaviour. The vertical expansion of the LNAPL distribution in such soils has two adverse effects with respect to the LNAPL mobility. First, more LNAPL becomes residual and second, the lower saturation of the

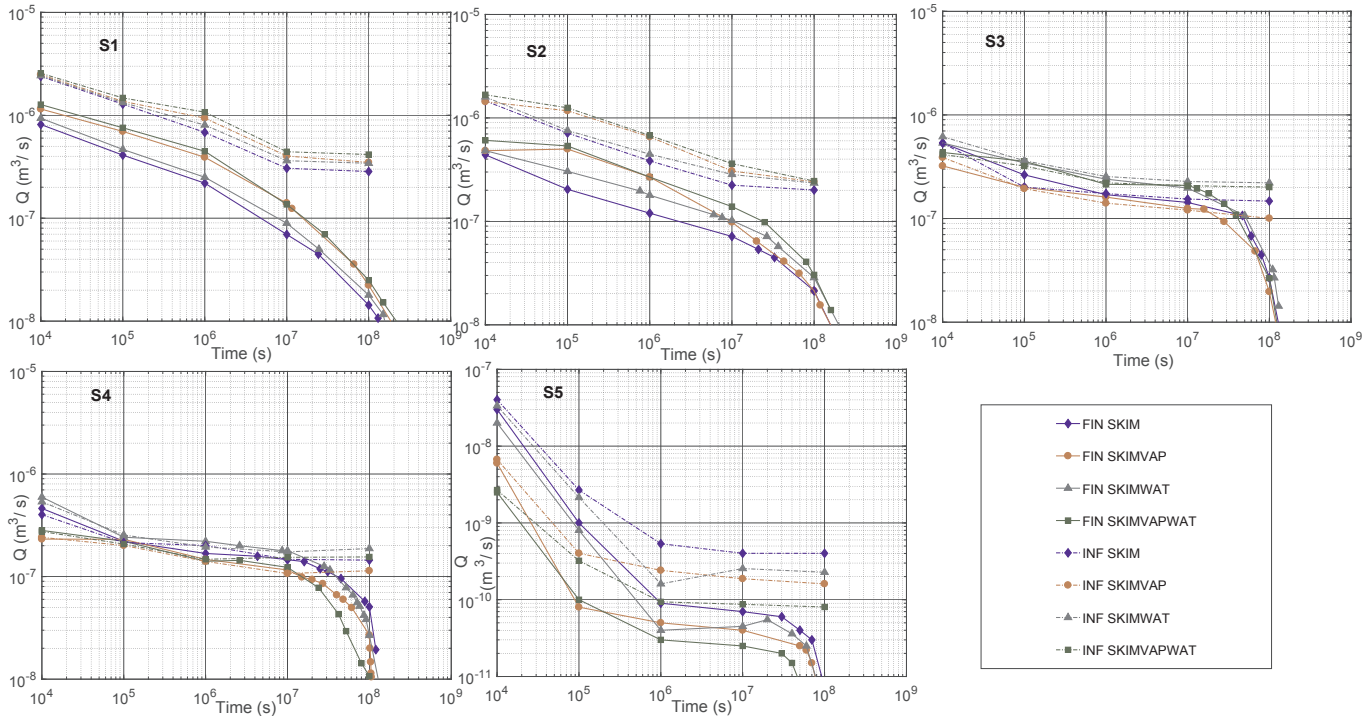


**Fig. 4.** H cases LNAPL recovery rates versus time.

LNAPL provides more void space increasing the air/water surface area and therefore, partitioning is increased. Both of these diminish the LNAPL mobility and therefore, the performance of skimming alone becomes more efficient (better LNAPL removal) as the soil becomes less permeable. Note that the figures show the rates of volumes of LNAPL recovered in liquid phase, and do not include mass removed in the vapour extracted from the well (this is discussed later).

The results suggest that if there is natural tendency for an inwards flux of the LNAPL towards the well following a remediation effort (here caused by the Dirichlet condition at the outer boundary), the volumetric recovery rate of LNAPL asymptotes to a certain value. A real-world case for such condition is a recovery well in a plume caused by an ongoing release of LNAPL. However, this asymptotic behaviour would not normally be apparent for steady or finite LNAPL plumes. The recovery rate would eventually decrease further (depending on the site and plume characteristics).

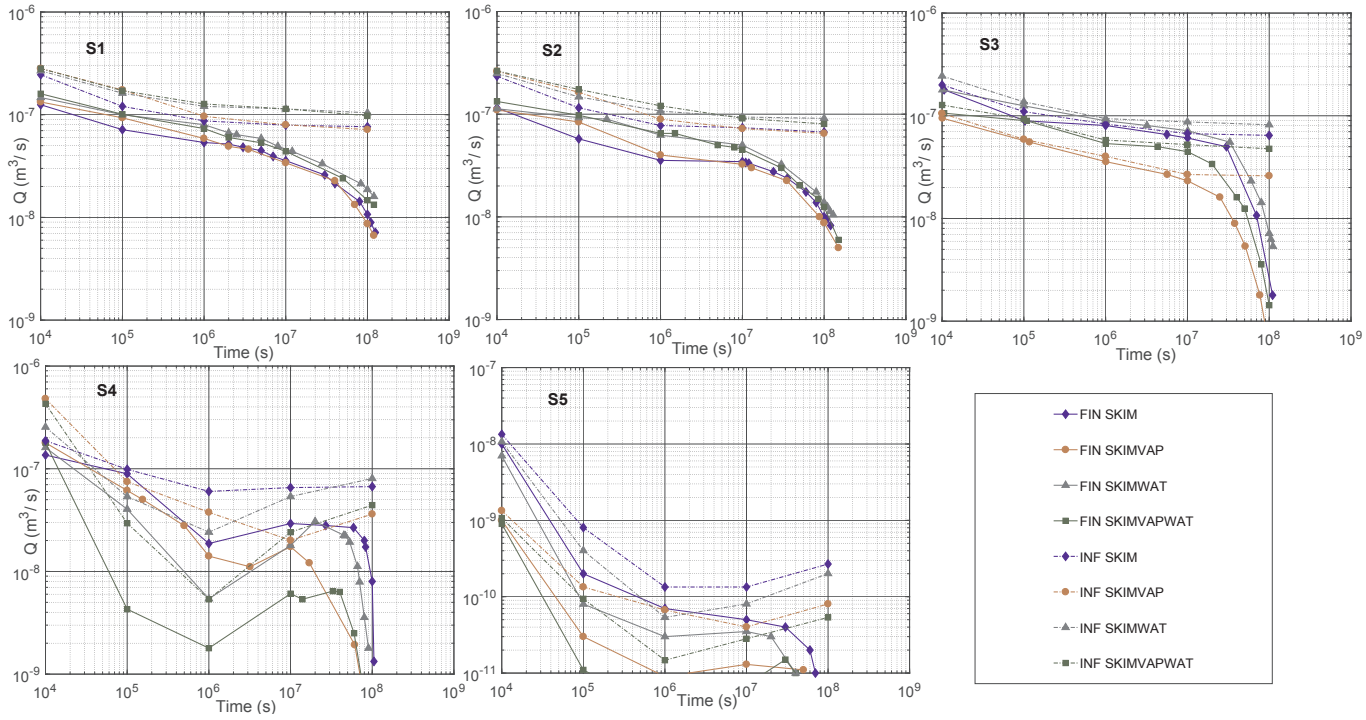


**Fig. 5.** L cases LNAPL recovery rate versus time.

#### 4.1.2. The finite LNAPL plume

The lower recovery rate set of simulations (solid lines) in Figs. 4 and 5 belong to the finite (FIN) cases. With an offset in the values, a general trend is that the FIN results follow the same trajectory of LNAPL recovery as for the infinite (INF) cases up to a certain time. Characteristically, this time is about $10^7$–$2 \times 10^7$ s (0.3–0.6 years). Beyond that time, the recovery rate for FIN cases decrease dramatically and generally by up to an order of magnitude over an order of magnitude of time (i.e., up to $10^8$–$2 \times 10^8$ s or ~3.2–6.3 years).

A steeper reduction in mass removal is seen for the less permeable soils. Interestingly, less disturbing approaches (e.g., skimming) seem to be able to recover at higher rates for longer in lower permeability soils, especially in FIN cases.

Determination of a remediation endpoint can be based on a range of factors. If we consider $10^{-8}$ $m^3$/s (equal to 0.86 l/day) as a reasonably low LNAPL recovery rate at which further recovery efforts might not be warranted (and the NSZD may become dominant), then for the H cases, the endpoint varies from 4 to 6 years for S1 to 3–4 years for S4. The recovery rates for S5 are much below this threshold after initial recovery efforts. For the L cases, the endpoint varies from almost 3–5 years for S1 to 2–3 years for S3. In S4, only the methods excluding vapour extraction remain above the endpoint threshold for more than one year.

Fig. 6 shows the cumulative recovered LNAPL volume in the liquid phase for the four most permeable soils. We excluded S5 as it failed to produce adequate volumes of recovered LNAPL (see Figs. 4 and 5). Recall that the total initial volume of LNAPL for the H and L cases were 33 $m^3$ and 6.6 $m^3$ respectively. Given this, the LNAPL recovered in the liquid phase after $10^8$ s (almost 3.2 years) varies from 14% to 30% of the initial volume for the H cases and 5%–53% for the L cases. Again it is seen that the performance of approaches including vacuum enhanced recovery for less permeable soils is not as efficient (as for the more permeable ones). S3 SKIMWAT produces the highest recovered LNAPL volumes. Despite the soil permeability in S3 being less than S1 and S2, the less horizontally-expanded LNAPL plume in this soil compensates for the inverse effect of the lower permeability. Therefore, and for a constant amount of LNAPL, the interaction between the LNAPL distribution and the soil permeability affects the recovery performance. This is observed in Fig. 7 where a snapshot of LNAPL saturation for FIN H S2-S4 SKIMVAPWAT is presented. It is seen that the horizontal expansion of the LNAPL plume for S2 is almost 50% higher than the counterpart value for S3.

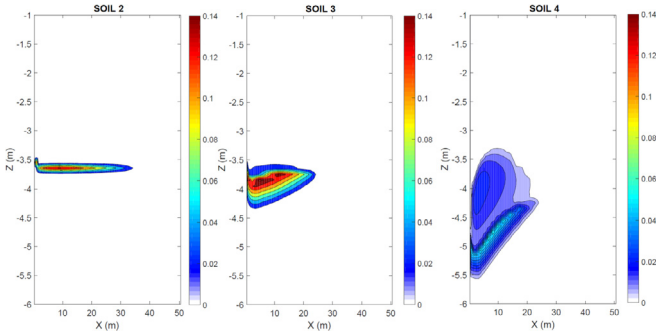


**Fig. 7.** The LNAPL saturation distribution after $10^8$ s (3.17 years) for FIN H S2-S4 SKIMVAPWAT cases.

Another observation in Fig. 6 is that SKIMVAPWAT (applying all techniques together) recovers the least LNAPL mass for S4. Indeed, the significantly-expanded vertical thickness of the LNAPL (see Fig. 7) in this case enhances volatilisation and immobilisation which in turn decreases recovery of the LNAPL liquid phase.

The LNAPL is also recovered in the gas phase. Fig. 8 shows the concentration of total volatile organic compounds (VOC) in the gas extracted from the well for the FIN-INF H-L SKIMVAP cases in S2 and S4. S2 was coarse enough to produce the 5 l/s of the extracted gas over the entire course of simulation. However, S4 only produced 0.23 l/s shortly after pumping started. In general, it is seen that the same asymptotic behaviour for the INF LNAPL recovery rates is also observed here. The concentrations for the FIN L cases start to deviate from the INF counterpart values earlier than the FIN H cases.

Considering the gas pumping rate and the concentrations, the three-year cumulative LNAPL volume recovered in the gas phase is 1.67 $m^3$

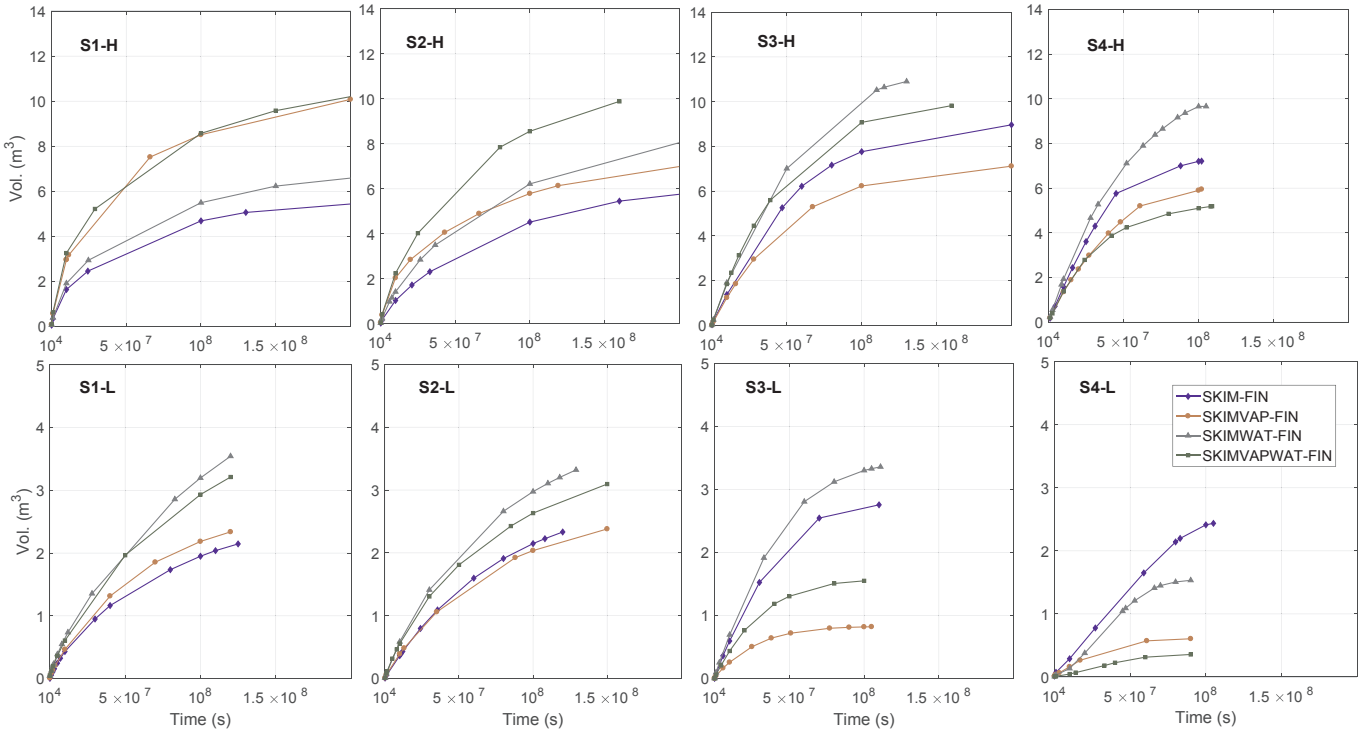


**Fig. 6.** The accumulative recovered LNAPL volume in the liquid phase for FIN cases.

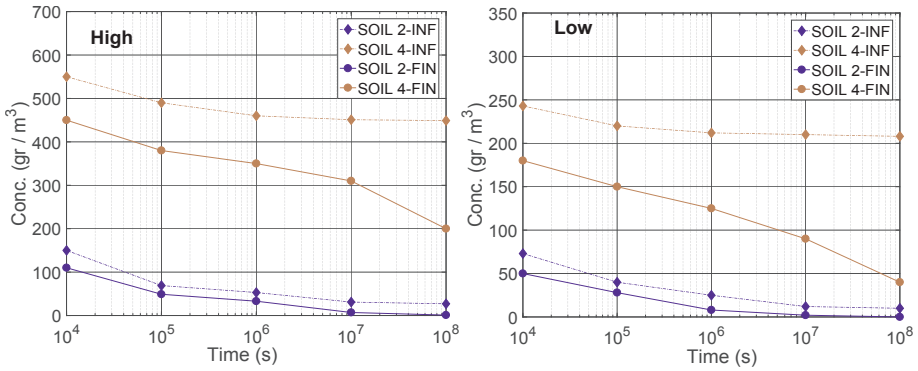


**Fig. 8.** Total volatile compound concentrations in the gas extracted in S2 and S4, H and L SKIMVAP cases.

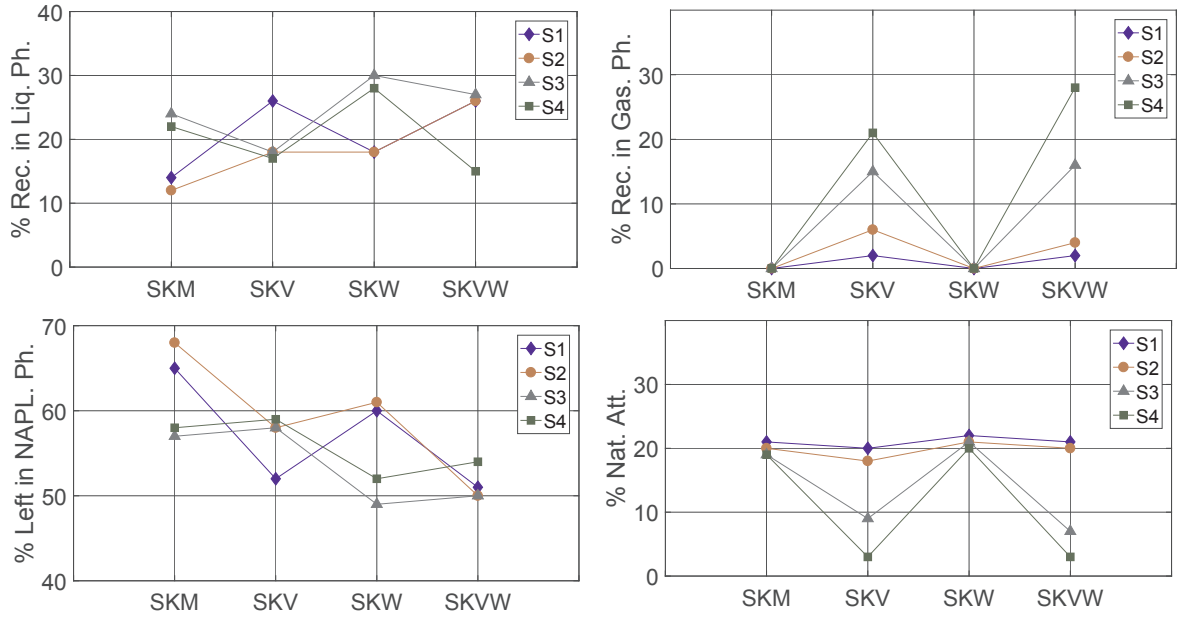


**Fig. 9.** From top left to bottom right, compared to the initial LNAPL mass and for FIN H cases; % recovered LNAPL in the liquid phase, % recovered LNAPL in the gaseous phase, % LNAPL left, % LNAPL lost due to natural attenuation (dissolution and natural evaporation).

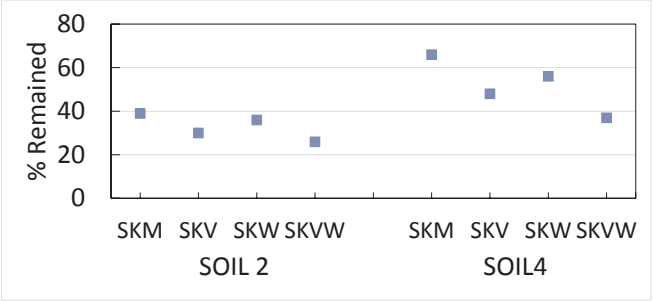


**Fig. 10.** % of the remained benzene in the LNAPL phase compared to its initial mass for FIN H cases.

and 6.9 $m^3$ for H S2 and H S4 cases and 0.44 $m^3$ and 2.41 $m^3$ for L S2 and L S4 cases respectively. It is noted that the recovered LNAPL percentage in the gas phase is higher for the L cases, mainly due to a greater available void space (and air/NAPL interfacial area) and therefore, a greater potential for volatilisation.

The recovered LNAPL mass in the aqueous phase was negligible. Indeed, the majority of the weathered gasoline sample used here includes NC46 and NC711 which have a very low solubility in water.

### 4.2. Mass balance

Fig. 9 summarizes the mass balance after $10^8$ s (3.2 years) for the S1-S4 cases. It includes the LNAPL mass percentage (in comparison to the initial LNAPL mass) recovered in the liquid and gas phase, the LNAPL mass percentage remaining and the LNAPL mass percentage lost due to natural volatilisation and dissolution. The same pattern in the order of the recovered LNAPL volume in the liquid phase in Fig. 6 is also seen here for the LNAPL mass left in the system.

For the less permeable soils (with a greater vertical LNAPL thickness and less horizontal LNAPL extent), the amount of LNAPL mass recovered in the gas phase is greater than more permeable soils. The LNAPL mass lost due to dissolution and natural volatilisation is less significant in such soils.

Hence vacuum enhanced recovery is more effective where the LNAPL mass is more vertically distributed in the vadose zone e.g., S4 (see Fig. 2). Fig. 9 shows that the cumulative LNAPL mass recovered in gas and liquid phases for S4 H SKIMVAP and S4 H SKIMVAPWAT is 38% and 43% respectively. Indeed, enhanced volatilisation of compounds like NC46, which are the most volatile and most abundant compounds in the LNAPL sample we study here, accounts for the majority of the mass recovered during vacuum-enhanced recovery in S4.

In addition to the recovery rate, other key factors in determining a non-biogenic endpoint are the remaining risks associated with

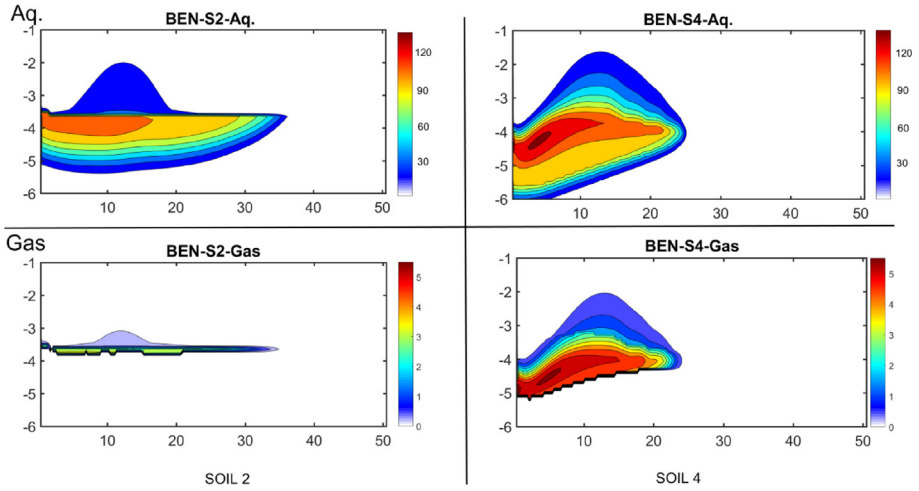


**Fig. 11.** Benzene concentration (gr/m$^3$) in aqueous (Aq. top row) and gaseous phase (bottom row) for FIN S2 and S4 SKIMVAPWAT.

hazardous chemicals remaining in the LNAPL and continuing to partition to water and vapour phases; and especially in comparison to the rate of NSZD (De Blanc, et al., 1996; Chaplin et al., 2002; Garg et al., 2017). Both of these are functions of the subsurface biochemical processes which are beyond the scope of this study but might be investigated with codes like TMVOCBio (Jung et al., 2017).

However, because of the risk profile of benzene (Aksoy, 1985) we provide some information on simulated benzene concentrations when approaching these LNAPL endpoints, to address the issue of technology effectiveness and soil/aquifer media types on reducing benzene concentrations.

Fig. 10 shows the remaining percentage of benzene in the LNAPL phase (compared to its initial mass in LNAPL) for (FIN H) S2 and S4. For the finer soil (S4), a significantly higher mass of benzene remains in the LNAPL compared to the coarser soil (S2) across all remediation types simulated (an average of 50% for S4 versus 30% for S2). As benzene is considerably volatile and soluble, enhanced natural volatilisation in the more permeable soil (S2) augments LNAPL benzene loss. This is more pronounced for technologies that include both water table drawdown and vapour extraction – together this induces a greater contact surface area between the LNAPL and aqueous and gaseous phases.

Fig. 11 shows concentrations of benzene in different phases after $10^8$ s for H S2, S4 SKIMVAPWAT. Overall, the concentration contours somewhat mimic the LNAPL architecture in Fig. 7, indicating potentially equilibrium conditions. Clearly, the significant effect of water table drawdown in S4 on the vertical extent of the LNAPL induces higher concentrations over a greater vertical thickness both in the gaseous and aqueous phases in the profile. The average concentration of benzene in the extracted soil gas was 0.01 and 1.06 g/m$^3$ for (FIN H SKIMVAPWAT) S2 and S4 respectively, with the total mass of benzene collected in the gaseous phase 7.0 and 24.6 kg respectively. This provides quantitative measures of the removal of highly hazardous LNAPL components like benzene using these approaches. The recovered benzene in the aqueous phase was negligible.

## 5. Conclusions

We conducted 80 representative multi-phase and multi-component scenario simulations to investigate the performance of various LNAPL recovery techniques. A wide range of soils, and LNAPL plume architectures and saturation were simulated in a recently verified parallel-processing simulation framework, based on TMVOC-MP.

For an infinitely large LNAPL plume there is a natural inwards flux of the LNAPL towards a recovery well (e.g., a recovery well in a plume caused by an ongoing release of LNAPL). As such, the volumetric recovery rate of LNAPL asymptotes to a constant value. For a finite plume, the recovered LNAPL mass in the liquid phase varied from 5% to 53%, but recovery rates at the end of similar extended simulation periods (3–6 years) were significantly lower than the asymptotic rates for the infinite LNAPL plume case. The LNAPL recovered in the gas phase for approaches including vapour extraction varied from 2% to 28%.

The primary aim of this research was to characterize a conservative (i.e. upper-limit) LNAPL recovery endpoint under various conditions. This was done by excluding biodegradation processes. Taking 0.86 l/day as an acceptably low recovery rate that may be taken as an endpoint, to achieve this took 2–6 years across the remedial options and for the conditions studied here. Including water table drawdown enhanced the vertical extent of the LNAPL and therefore, greater concentrations were observed in gaseous and aqueous phases. Because of its hazard nature, benzene removal and persistence was also investigated for selected scenarios.

Results from the 80 scenarios (in particular Figs. 4 and 5) provide a basis to estimate recovery endpoints for similar conditions, and a basis for halting or continuance of engineered LNAPL remedial efforts at sites. Different degrees of weathering, viscosity and partitioning attributes of the compounds as well as applying multiple recovery wells may alter the findings. The study showed that by using appropriate computational resources, it is possible to accurately assess the effectiveness of complex groundwater and LNAPL remedial and recovery methods under various site conditions. Using more-advanced multi-phase multi-component codes (e.g., parallel TMVOCBio (Jung et al., 2017)), it may be possible to additionally quantify biodegradation contributions to mass depletion (in particular for approaches with induced subsurface air flow) which would also allow more reliable estimation of compound-specific concentrations and exposures to conduct risk assessments for site closure considerations.

## Acknowledgments

The work has been supported by the Cooperative Research Centre for Contamination Assessment and Remediation of the Environment (CRC CARE), whose activities are funded by the Australian Governments Cooperative Research Centres Programme. It was also supported by resources provided by the Pawsey Supercomputing Centre with funding from the Australian Government and the Government of Western Australia and also the resources at CSIRO Pearcey cluster.

## References


Aksoy, M., 1985. Benzene as a leukemogenic and carcinogenic agent. Am. J. Ind. Med. 8, 9–20.

Barry, D.A., Prommer, H., Miller, C.T., Engesgaard, P., Brun, A., Zheng, C., 2002. Modelling the fate of oxidisable organic contaminants in groundwater. Adv. Water Resour. 25, 945–983.

De Blanc, P.C., McKinney, D.C., Speitel, G.E., 1996. Chapter 1 Modeling subsurface biodegradation of non-aqueous phase liquids. In: Corapcioglu, M.Y. (Ed.), Advances in Porous Media. Elsevier, pp. 1–86.

Carsel, R.F., Parrish, R.S., 1988. Developing joint probability distributions of soil water retention characteristics. Water Resour. Res. 24, 755–769.

Chaplin, B.P., Delin, G.N., Baker, R.J., Lahvis, M.A., 2002. Long-term evolution of biodegradation and volatilization rates in a crude oil-contaminated aquifer. Ann. Finance 6, 237–255.

Charbeneau, R.J., Johns, R.T., Lake, L.W., McAdams III, M.J., 2000. Free-Product recovery of petroleum hydrocarbon liquids. Groundwater Monit. Remediation 20, 147–158.

Davis, G.B., Ryner, J.L., Tregry, M.G., Fisher, S.J., Patterson, B.M., 2005. Measurement and modeling of temporal variations in hydrocarbon vapor behavior in a layered soil profile. Vadose Zone J. 4, 225–239.

Davis, G.B., Patterson, B.M., Trefry, M.G., 2009. Evidence for instantaneous oxygen-limited biodegradation of petroleum hydrocarbon vapors in the subsurface. Groundwater Monit. Remediation 29, 126–137.

Davis, G.B., Laslett, D., Patterson, B.M., Johnston, C.D., 2013. Integrating spatial and temporal oxygen data to improve the quantification of in situ petroleum biodegradation rates. J. Environ. Manag. 117, 42–49.

DiFilippo, E.L., Brusseau, M.L., 2008. Relationship between mass-flux reduction and source-zone mass removal: analysis of field data. J. Contam. Hydrol. 98, 22–35.

Gabr, M.A., Sharmin, N., Quaranta, J.D., 2013. Multiphase extraction of light non-aqueous phase liquid (LNAPL) using prefabricated vertical wells. Geotech. Geol. Eng. 31, 103–118.

Garg, S., Newell, C.J., Kulkarni, P.R., King, D.C., Adamson, D.T., Renno, M.I., Sale, T., 2017. Overview of natural source zone depletion: processes, controlling factors, and composition change. Groundwater Monit. Remediation 37, 62–81.

GSI Environmental Inc, 2012. BioVapor a 1-D Vapor Intrusion Model with Oxygen-limited Aerobic Biodegradation. API, Houston.

Hernández-Espriú, A., Martínez-Santos, P., Sánchez-León, E., Marín, L.E., 2012. Free-product plume distribution and recovery modeling prediction in a diesel-contaminated volcanic aquifer. Phys. Chem. Earth 37–39, 43–51.

Huntley, D., Beckett, G.D., 2002. Persistence of LNAPL sources: relationship between risk reduction and LNAPL recovery. J. Contam. Hydrol. 59, 3–26.

Jeong, J., Charbeneau, R.J., 2014. An analytical model for predicting LNAPL distribution and recovery from multi-layered soils. J. Contam. Hydrol. 156, 52–61.

Johnson, P.C., Lundegard, P.D., Liu, Z., 2006. Source zone natural attenuation at petroleum hydrocarbon spill sites—I: site-specific assessment approach. Groundwater Monit. Remediation 26.

Johnston, C.D., Trefry, M.G., 2009. Characteristics of light nonaqueous phase liquid recovery in the presence of fine-scale soil layering. Water Resour. Res. 45, W05412.

Johnston, C.D., Fisher, S., Rayner, J.L., 2001. Removal of Petroleum Hydrocarbons from the Vadose Zone During Multi-phase Extraction at a Contaminated Industrial Site. IAHS, Sheffield.

Johnston, C.D., Davis, G.B., Bastow, T.P., Annable, M.D., Trefry, M.G., Furness, A., Gaste, Y., Woodbury, R.J., Rao, P.S.C., Rhodes, S., 2013. The use of mass depletion-mass flux reduction relationships during pumping to determine source zone mass of a reactive brominated-solvent DNAPL. J. Contam. Hydrol. 144, 122–137.

Jung, Y., Pau, G.S.H., Finsterle, S., Pollyea, R.M., 2017. TOUGH3: a new efficient version of the TOUGH suite of multiphase flow and transport simulators. Comput. Geosci. 108, 2–7.

Kaplan, I.R., Galperin, Y., Lu, S., Lee, R., 1997. Forensic Environmental Geochemistry: differentiation of fuel-types, their sources and release time. Org. Geochem. 27, 289–299.

Khan, F.I., Husain, T., Hejazi, R., 2004. An overview and analysis of site remediation technologies. J. Environ. Manag. 71, 95–122.

Lang, D., et al., 2009. Polar compounds from the dissolution of weathered diesel. Ground Water Monit. Remediation 29, 85–93.

Lekmine, G., Sookhak Lari, K., Johnston, C.D., Bastow, T.P., Rayner, J.L., Davis, G.B., 2017. Evaluating the reliability of equilibrium dissolution assumption from residual gasoline in contact with water saturated sands. J. Contam. Hydrol. 196, 30–42.

Lenhard, R.J., Sookhak Lari, K., Rayner, J.L., Davis, G.B., 2018. Evaluating an analytical model to predict subsurface LNAPL distributions and transmissivity from current and historic fluid levels in groundwater wells: comparing results to numerical simulations. Ground water Monit. Remediation 38, 75–84. https://doi.org/10.1111/gwmr.12254. (Volume Accepted).

Mulligan, C.N., Yong, R.N., 2004. Natural attenuation of contaminated soils. Environ. Int. 30, 587–601.

Parker, J.C., Lenhard, R.J., Kuppusamy, T., 1987. A parametric model for constitutive properties governing multiphase flow in porous media. Water Resour. Res. 23, 618–624.

Prommer, H., Barry, D.A., Davis, G.B., 2000. Numerical modelling for design and evaluation of groundwater remediation schemes. Ecol. Modell. 128, 181–195.

Pruess, K., Battistelli, A., 2002. TMVOC, a Numerical Simulator for Three-phase Non-isothermal Flows of Multicomponent Hydrocarbon Mixtures in Saturated-unsaturated Heterogeneous Media. Berkeley, CA 94720, U.S.A.: s.n.

Rivett, M.O. (Ed.), 2014. An Illustrated Handbook of LNAPL Transport and Fate in the Subsurface. AIRE, London s.l.:CL.

Skinner, A.M., 2013. LNAPL Longevity as a Function of Remedial Actions: Tools for Evaluating LNAPL Remedies. (s.l.: s.n).

Sookhak Lari, K., Johnston, C.D., Davis, G.B., 2015. Interfacial mass transport in porous media augmented with bulk reactions: analytical and numerical solutions. Transport Porous Media 106, 405–423.

Sookhak Lari, K., Davis, G.B., Johnston, C.D., 2016a. Incorporating hysteresis in a multi-phase multi-component NAPL modelling framework; a multi-component LNAPL gasoline example. Adv. Water Res. 96, 190–201.

Sookhak Lari, K., Johnston, C.D., Davis, G.B., 2016b. Gasoline multi-phase and multi-component partitioning in the vadose zone: dynamics and risk longevity. Vadose Zone J. 15, 1–15.

Sookhak Lari, K., Johnston, C.D., Rayner, J.L., Davis, G.B., 2018. Field-scale multi-phase LNAPL remediation: validating a new computational framework against sequential field pilot trials. J. Hazard. Mater. 345, 87–96.

Vasudevan, M., Johnston, C.D., Bastow, T.P., Lekmine, G., Rayner, J.L., Nambi, I.M., Suresh Kumar, G., Ravi Krishna, R., Davis, G.B., 2016. Effect of compositional heterogeneity on dissolution of non-ideal LNAPL mixtures. J. Contam. Hydrol. 194, 10–16.

Zhang, K., Yamamoto, H. & Pruess, K., 2007. TMVOC-MP: a Parallel Numerical Simulator for Three Phase Non-isothermal Flows of Multicomponent Hydrocarbon Mixtures in Porous/Fractured Media, (s.l.: s.n).